

## Supplementary Information

### Emergence of Multicolor Photoluminescence in $\text{La}_{0.67}\text{Sr}_{0.33}\text{MnO}_3$ Nanoparticles

Anupam Giri <sup>a</sup>, Nirmal Goswami <sup>a</sup>, M. S. Bootharaju <sup>b</sup>, Paulrajpillai Lourdu Xavier <sup>b</sup>, Robin John <sup>b</sup>, Nguyen T. K. Thanh <sup>c,d</sup>, Thalappil Pradeep <sup>b</sup>, Barnali Ghosh <sup>a</sup>, Arup K. Raychaudhuri <sup>a</sup> and Samir K. Pal <sup>a\*</sup>

<sup>a</sup>*Unit for Nano Science and Technology, S. N. Bose National Centre for Basic Sciences, Block JD, Sector III, Salt Lake, Kolkata 700 098, India*

<sup>b</sup>*Department of Chemistry, Indian Institute of Technology Madras, Chennai 600 036 India*

<sup>c</sup>*Department of Physics and Astronomy, University College London, Gower Street, London WC1E 6BT, United Kingdom*

<sup>d</sup>*The Davy-Faraday Research Laboratory, The Royal Institution of Great Britain, 21 Albemarle Street, London, W1S 4BS, United Kingdom*

\*Corresponding Authors Email: [skpal@bose.res.in](mailto:skpal@bose.res.in)

## 1. Magnetic study of Tartrate-LSMO NPs

In case of as-prepared LSMO NPs, simultaneous electron transfer between  $\text{Mn}^{3+}$  and  $\text{Mn}^{4+}$  ions via an oxygen ion (i.e. exchange between  $\text{Mn}^{3+}$  and  $\text{Mn}^{4+}$  ions, well known as *double exchange*) plays the key role for the origin of their room temperature ferromagnetism<sup>1</sup>. So, any perturbation to the parallel alignment of the spins of the two adjacent cations or if the  $\text{Mn}^{3+}$ -O- $\text{Mn}^{4+}$  bond is bent, the electron transfer becomes more difficult and the magnetic interaction decreases. The magnetization of T-LSMO NPs was measured using superconducting quantum interference device (SQUID) magnetometry and the NPs showed paramagnetic behavior at low temperature (upto 50 K), while they were diamagnetic at around room temperature (shown in Supporting Information Figure S10). Thus, upon functionalization with tartrate the magnetic behavior of LSMO NPs has been changed dramatically from room temperature ferromagnetic to diamagnetic. This flipping of magnetism could be due to small average size ( $\sim 4$  nm, see Figure 5d of main text ) of the T-LSMO NPs (as tartrate only solubilized the small sized particles out of a wide range of particle size from 2 to 30 nm in the as-prepared LSMO NPs) or due to any distortion of the  $\text{Mn}^{3+}$ -O- $\text{Mn}^{4+}$  bond.

## 2. Incorporation of Tartrate-LSMO NPs into human oral squamous epithelial cells

The observed phenomena that there can be multiple photoluminescence from the T-LSMO, has been utilized for investigating possible *in vitro* cells imaging. Importantly, this has been done by employing the intrinsic photoluminescent properties of T-LSMO NPs, without further grafting of any biorecognition molecules (e.g., oligonucleotides, antibodies, or peptides) onto the NP surface. In this study, a primary squamous epithelial cells collected from the inner lining of human mouth have been used. Prior to cell imaging, the cells were spread on glass slides in presence of PBS (phosphate buffered saline) and NP solution (at a final concentration of  $3 \times 10^{-6}$

M) was added followed by 30 min of incubation. After incubation, the cells were washed twice with PBS to remove unbound NPs. Figure S11 demonstrates the fluorescence microscopic images of the cell labeled with T-LSMO NPs. Upper left image in the figure represent the bright-field images (black arrows indicate the nucleus of the cell) and other three images represent fluorescence images (employing 365, 436 and 546 nm excitation wavelengths respectively) of the T-LSMO NP labeled cells. Our results show that in case of NP treated cells, all fluorescence of the NPs (365, 436 and 546 nm excitation wavelength) are preferentially derived from the nuclear region of the cells. To verify the sub-cellular localization of the NPs in the cells, double labeling experiments using NPs and other fluorescent organelle marker in a single set of cell was not possible, as the excitation wavelengths of the NPs matched with that of the marker. Therefore, to circumvent this problem, we have done localization experiments with NPs and fluorescent nuclear marker (DAPI) in separate sets of cells (Figure S12). The comparative evaluation of the results from these two set of experiments suggest that the particles were indeed in the nucleus. The control image (Figure S13) shows no fluorescence from untreated squamous epithelial cells compared to those with incorporated T-LSMO NPs (Figure S11). The efficiency of cellular internalization and subsequent nuclear localization of T-LSMO NPs has also been revealed from time-dependent cellular uptake experiment (Figure S14) by monitoring (using fluorescence microscope and excitation wavelength of 365 nm) a single set of cell for 30 min after addition of the NPs. As shown in the figure, within 30 min, the NPs become enriched inside the nucleus of the cells. Although, the cellular internalization of untargeted negatively charged (due to carboxylate groups of tartrate) NPs is believed to occur through nonspecific binding on cationic sites of the plasma membrane followed by their endocytosis<sup>2</sup>, the reason behind their efficient nuclear localization is unknown and needs further rigorous investigation. However,

taken together these multicolor photoluminescence and efficient nuclear localization results suggest that the T-LSMO NP has the potential for multifunctional nanoprobe in terms of biological imaging and targeted drug delivery. According to a recent study liquid extract of LSMO nanoparticles are not toxic to the cells<sup>3</sup> and we have also found that T-LSMO NPs are nontoxic by a standard MTT cell viability assay (data not shown).

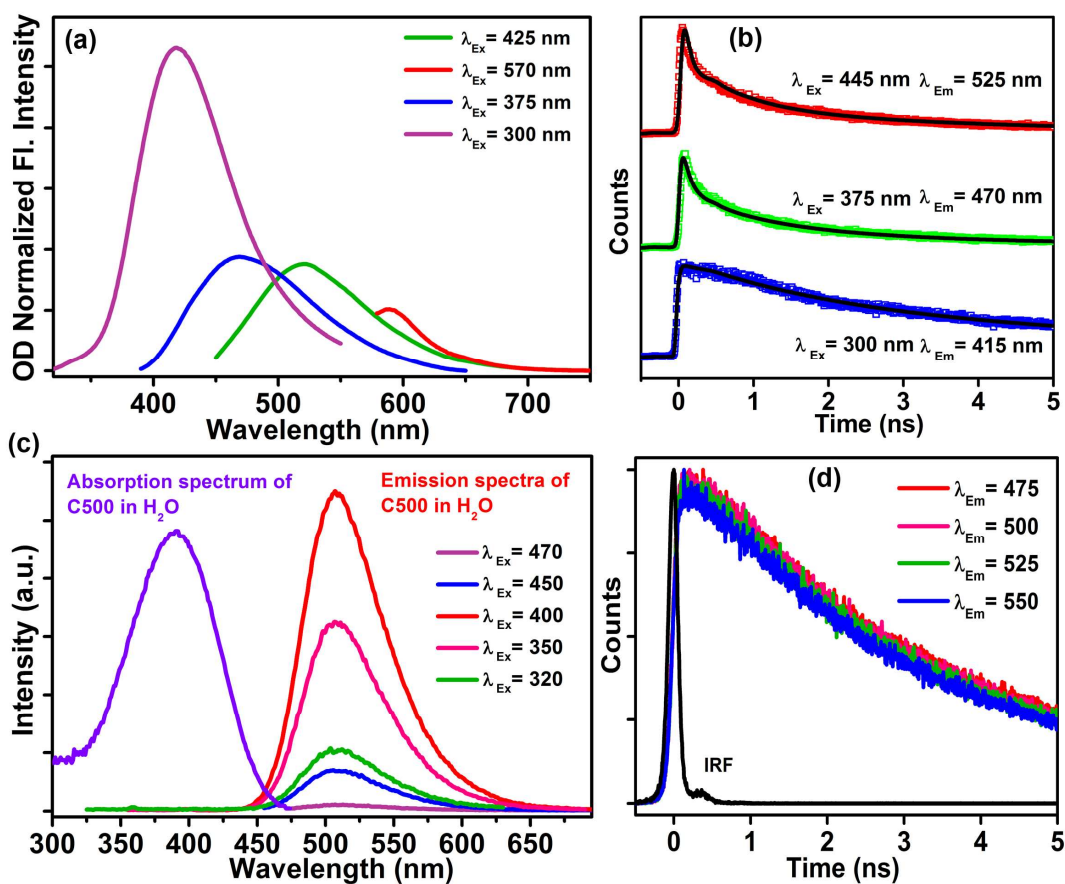


**Figure S1.** a) OD normalized PL spectra of Tartrate-LSMO NPs at pH~7. b) Picosecond-resolved photoluminescence decays transients of tartrate-LSMO NPs in water measured at emission wavelengths of 415, 470 and 525 nm upon excitation with laser source of 300, 375 and 445 nm wavelengths respectively. c) Absorption spectrum and excitation wavelength dependent emission spectra of C500 in water. The emission spectra show unique characteristics (position of the emission peak and spectral width) independent of the wavelength of excitation. d) Picosecond-resolved photoluminescence decays transients of C500 in water measured at emission wavelengths of 475, 500, 525 and 550 nm upon excitation with a laser source of 375 nm wavelength. The transients detected at various emission wavelengths show similar decay constants of 2.77 ns (51.61%) and 4.37 ns (48.38%).

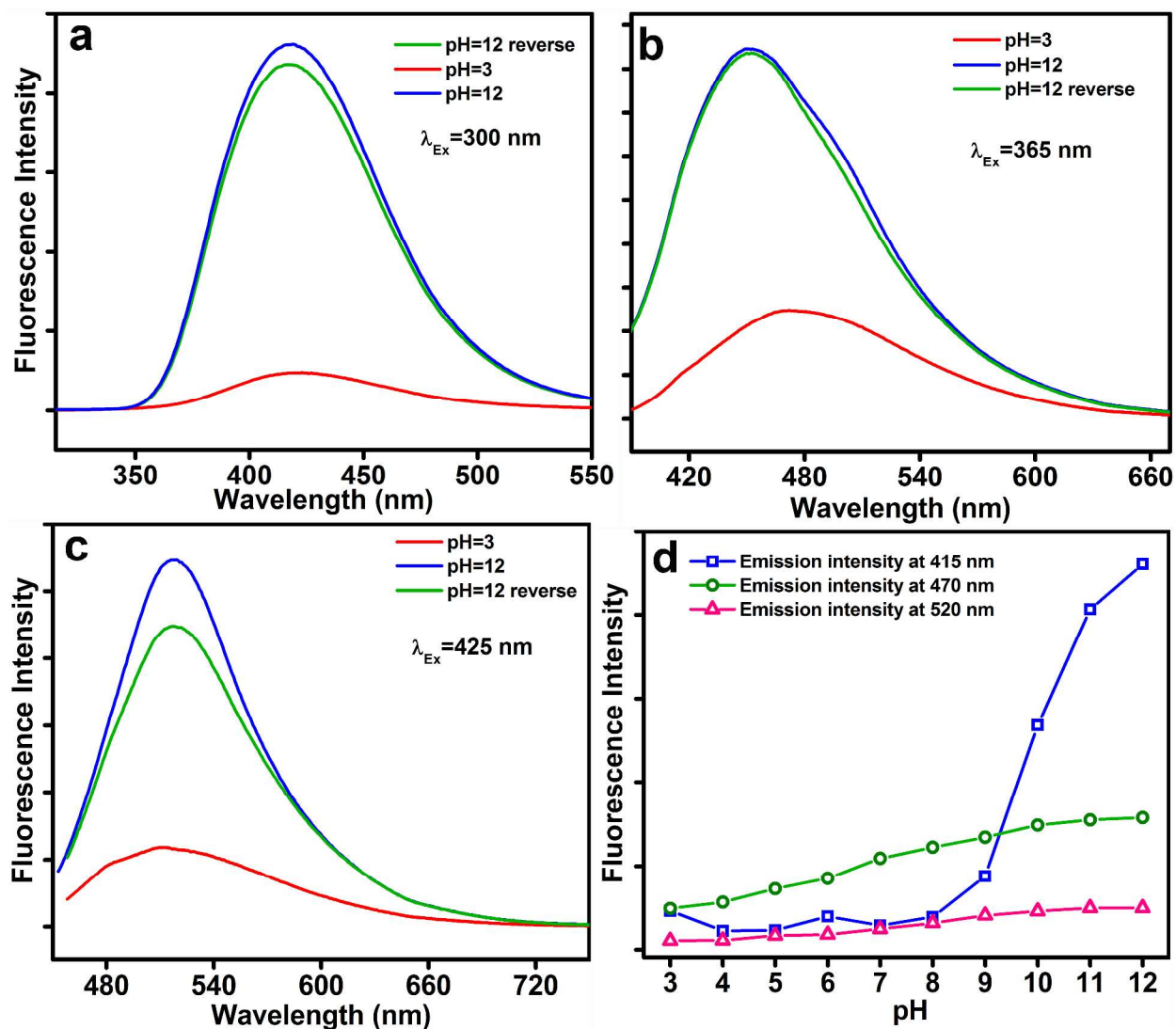


**Figure S2.** pH dependent photoluminescence (PL) spectra of T-LSMO NPs. a), b) and c) Represents the photoluminescence quenching and recovery of T-LSMO NPs by changing the pH of the solution from 12 (blue spectrum) to 3 (red spectrum) and again reverse back to 12 (green spectrum). d) Represents the change of PL intensity at different PL maximum with changing the pH of the solution from 12 to 3 by drop wise addition of HCl. Solid lines are a guide to the eye.

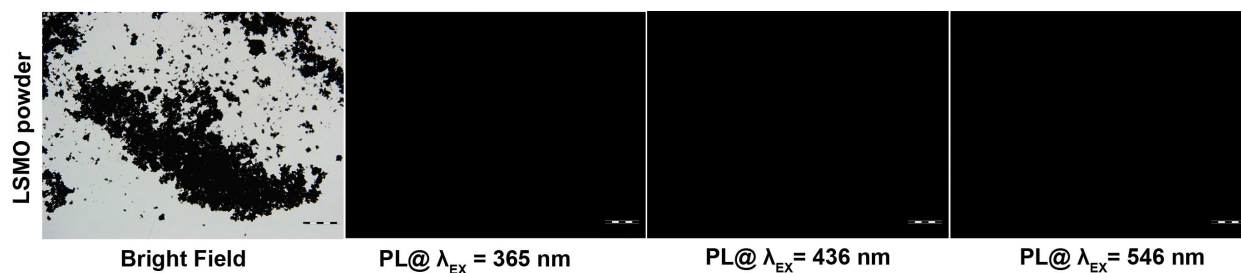


**Figure S3.** Fluorescence microscopic images of as-prepared LSMO NPs powder under irradiation of white light (bright field) and light of three different wavelengths of 365, 436 and 546 nm.

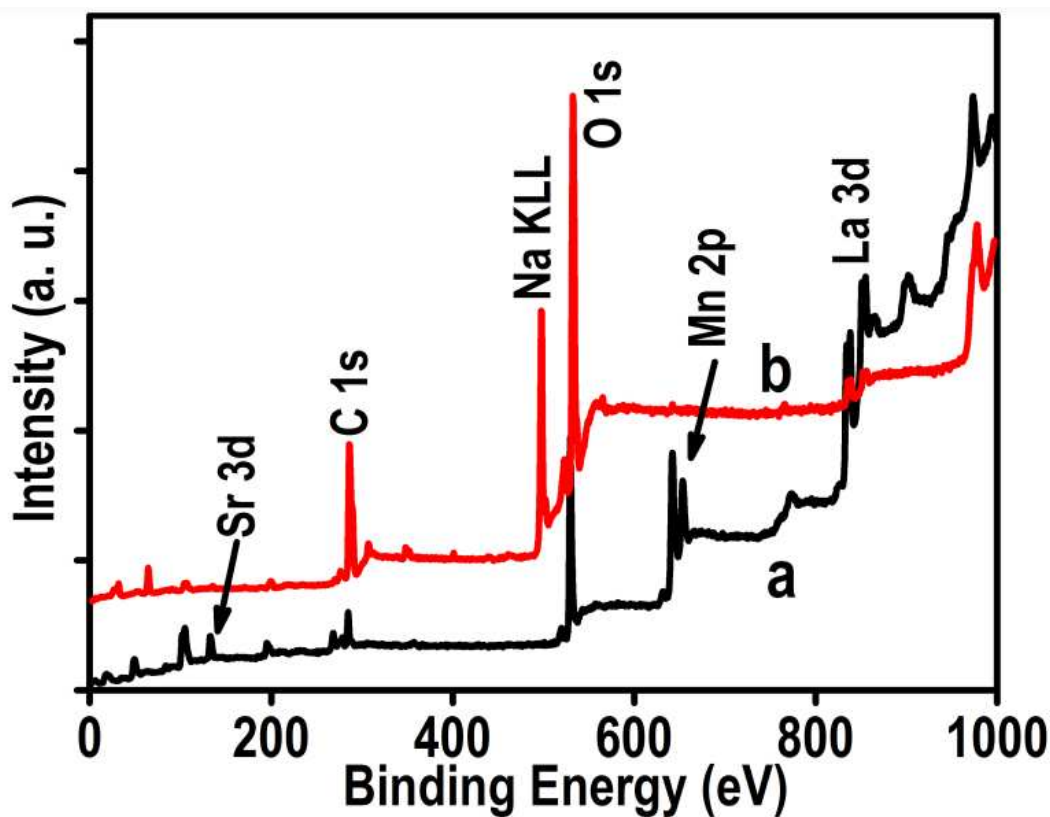


**Figure S4.** XPS survey spectra of LSMO NPs (traces a) and T-LSMO NPs (traces b) showing the expected elements.

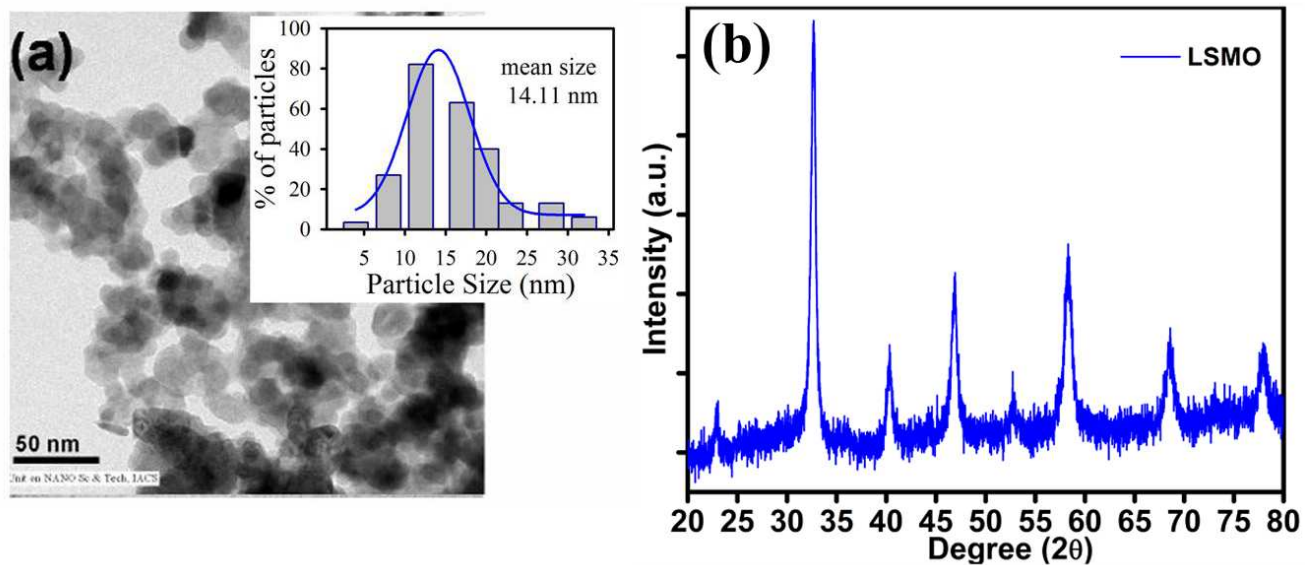


**Figure S5.** (a) Represents the TEM image of the as prepared LSMO NPs and the inset showing the particle size distribution. (b) Shows XRD pattern of as-prepared bulk LSMO NPs and the corresponding peak positions matched with the values reported earlier.

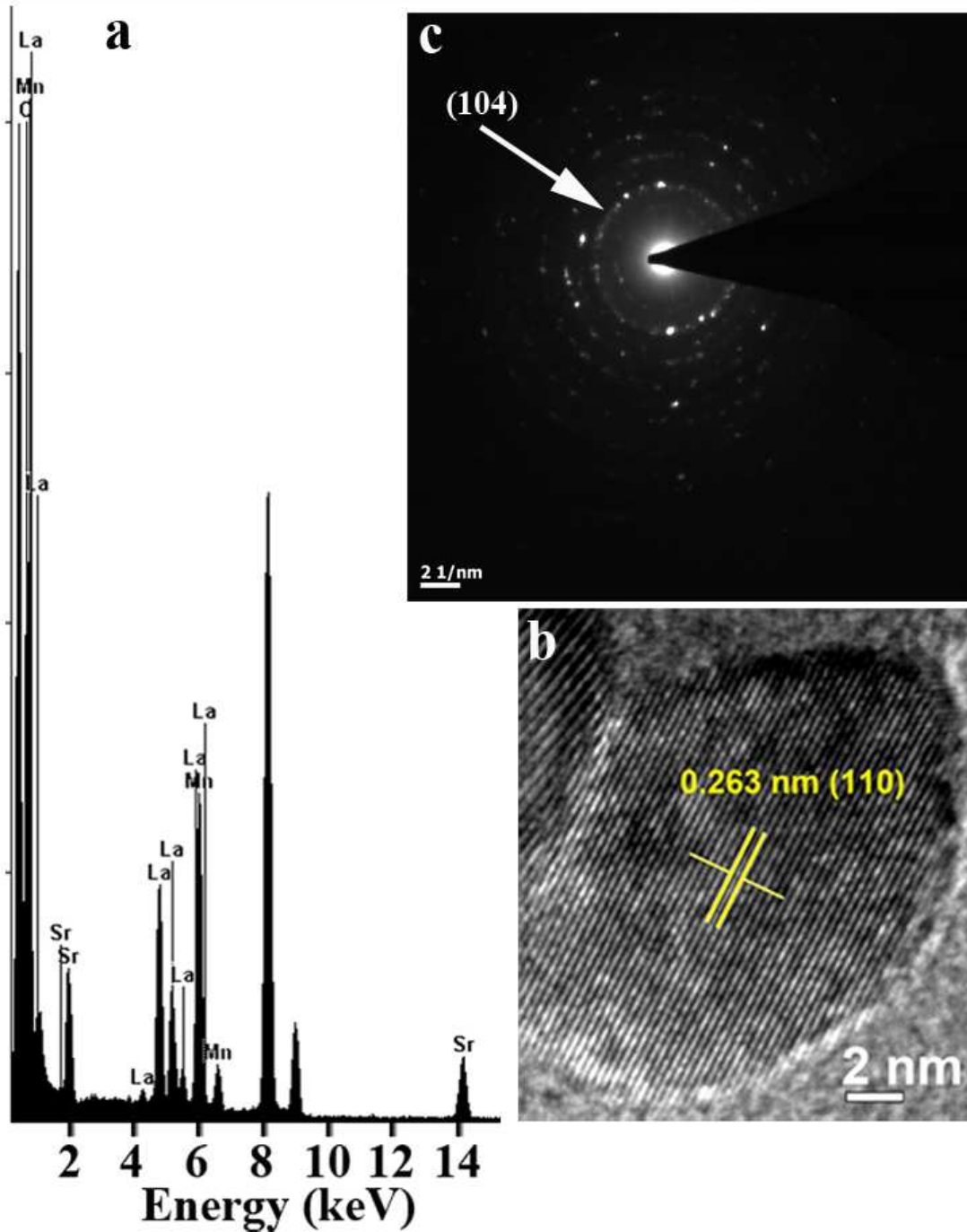


**Figure S6.** (a) The EDAX spectrum of as prepared LSMO NPs shows elemental composition of the NPs. (b) HRTEM image of as-prepared LSMO NPs having interplanar distance of 0.263 nm (which is similar with Tartrate-LSMO NPs shown in main text Figure 5e) corresponding to (110) plane of the crystal lattice. (c) SAED pattern of the as prepared LSMO NPs and the arrow head indicates the diffraction ring originated from (104) plane of the crystal lattice.

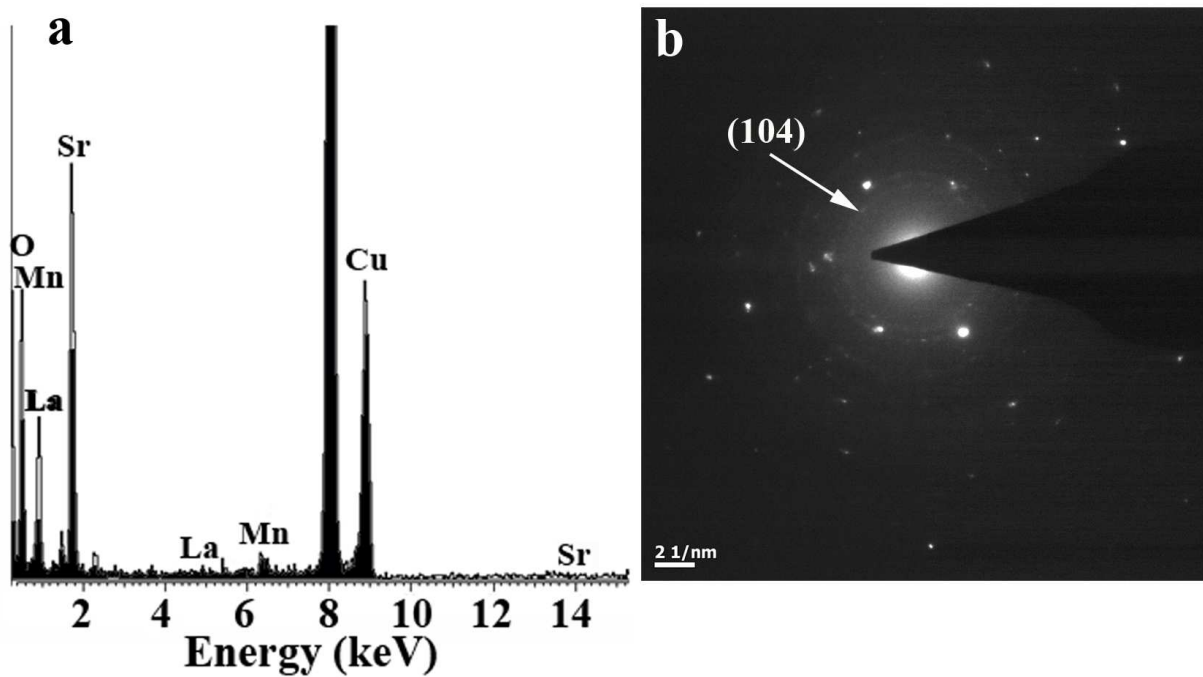


**Figure S7.** (a) The EDAX spectrum of Tartrate-LSMO NPs shows elemental composition of the NPs. (b) SAED pattern of the Tartrate-LSMO NPs. Arrow head indicates the appearance of diffraction ring from (104) plane, which have also been observed in case of as prepared LSMO NPs shown in Figure S6c.

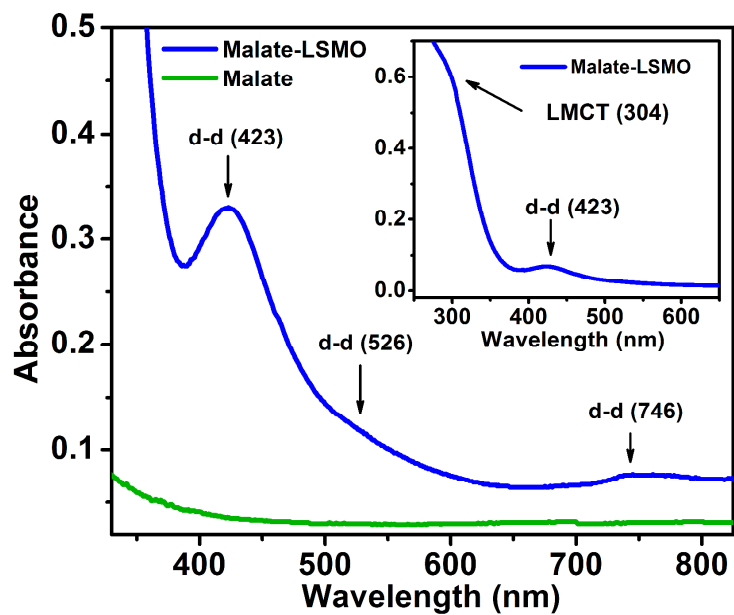


**Figure S8.** UV-vis absorption spectrum of malate and malate-LSMO NPs in aqueous solution at pH~7. Inset shows the absorption peak (LMCT) at around 304 nm obtained from diluted solution of malate-LSMO NPs.

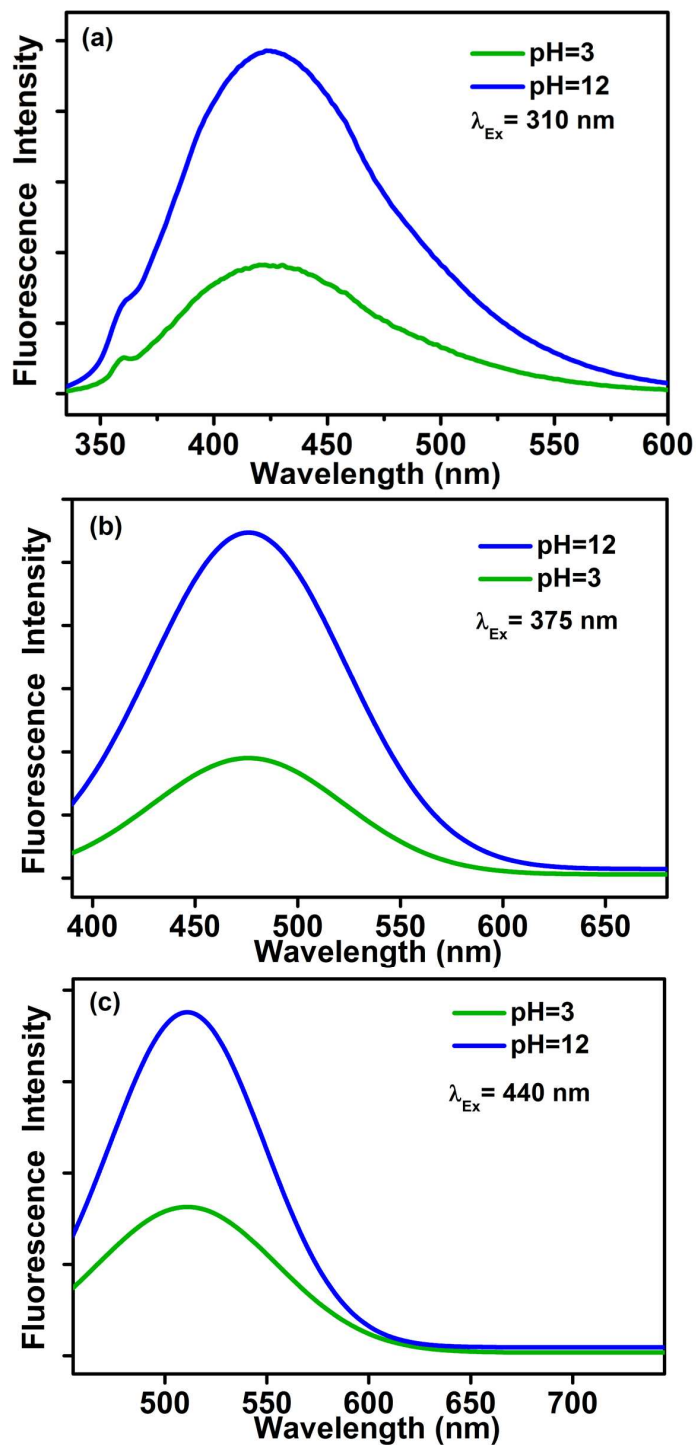


**Figure S9.** pH dependent photoluminescence (PL) spectra of Citrate-LSMO NPs. a), b) and c) represents the photoluminescence quenching of Citrate-LSMO NPs by changing the pH of the solution from 12 (blue spectrum) to 3 (green spectrum).

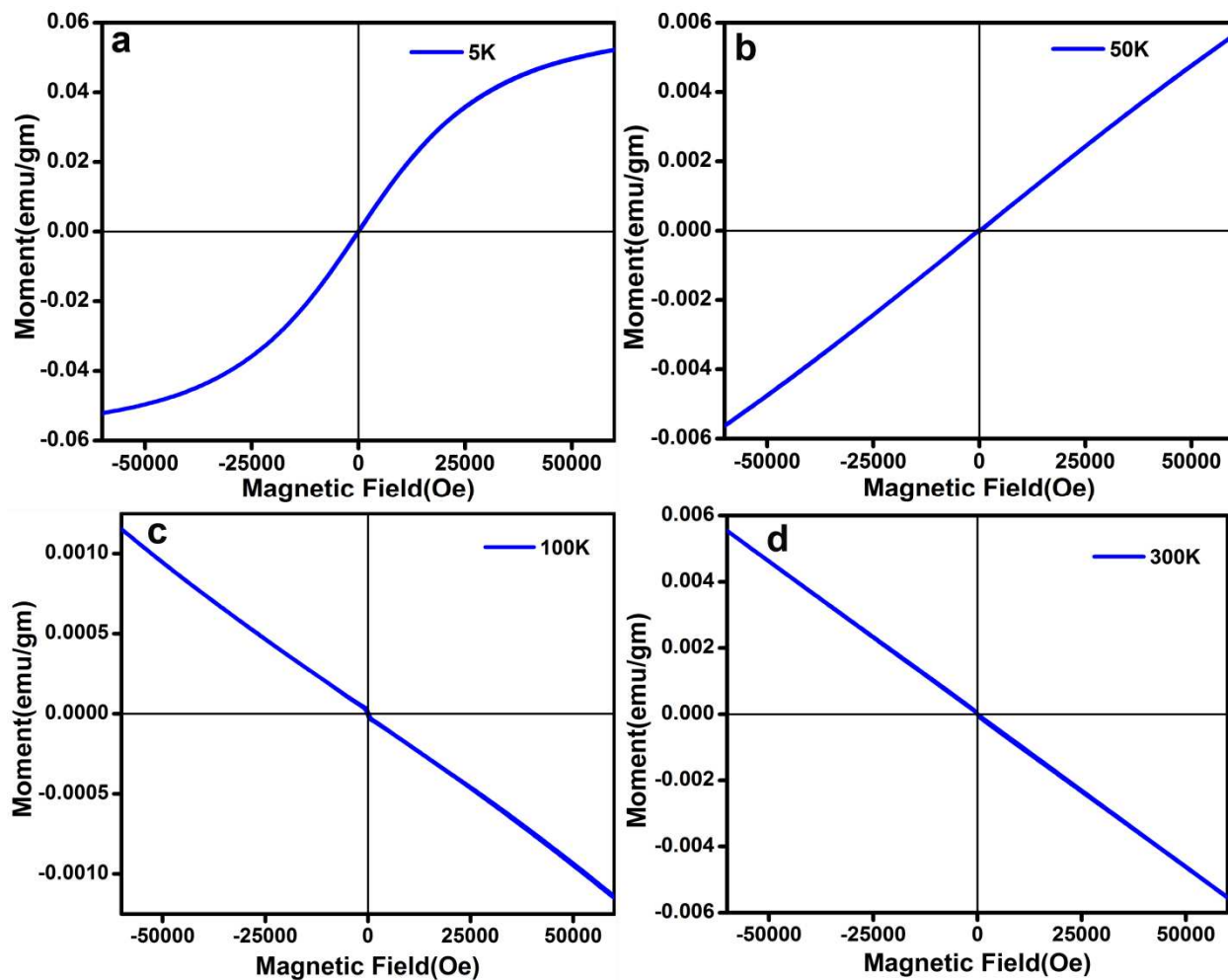


**Figure S10.** The M (moment)-H (magnetic field applied) magnetization plots of T-LSMO NPs at different temperature.

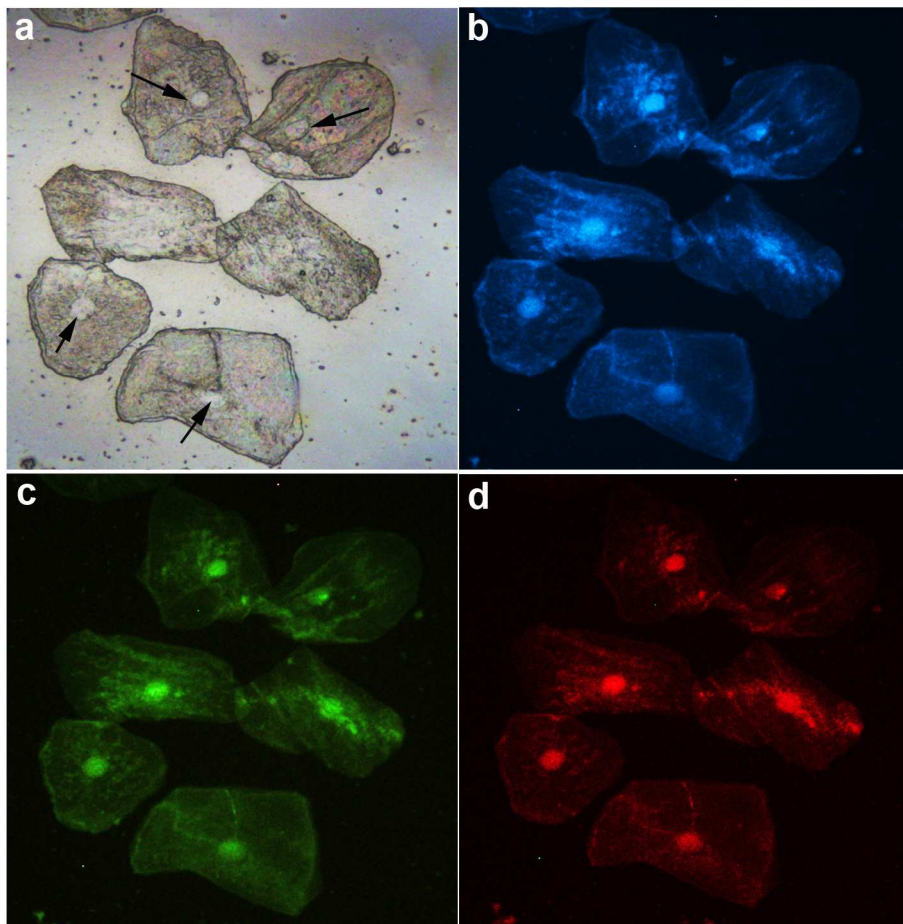


**Figure S11.** Representative fluorescence microscopic images of human oral squamous epithelial cells labeled with T-LSMO NPs. Upper left image corresponds to the bright-field image of the cells and the black arrows indicate the nucleus of the cells. The fluorescence images were taken using 365 (b), 436 (c) and 546 nm (d) excitations wavelengths. Selective nuclear localization of the NPs is clearly evident from the multicolor photoluminescence images of the cell.

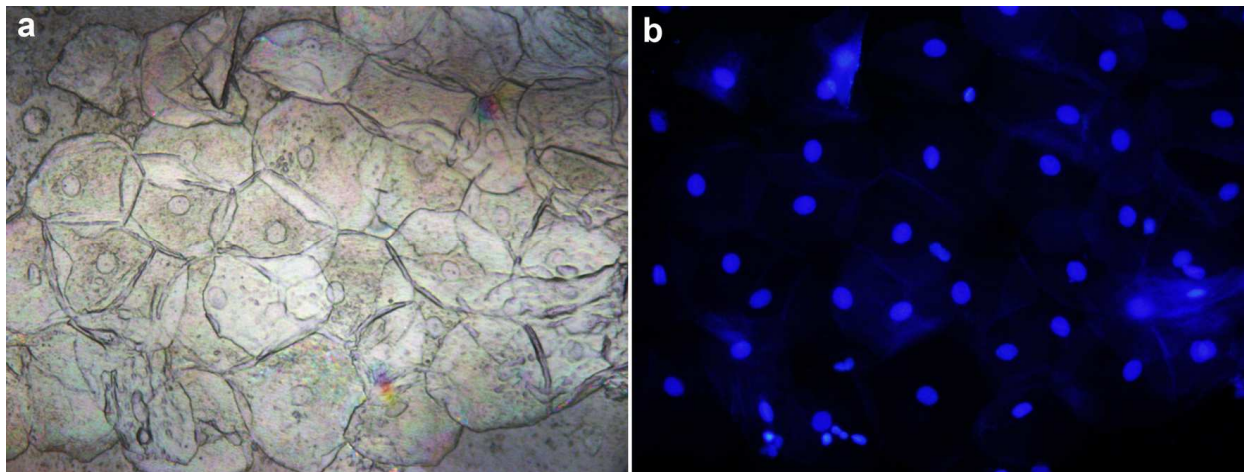


**Figure S12.** (a) Bright-field image of human oral squamous epithelial cells and (b) fluorescence micrographs (using an excitation source of 365 nm wavelength) of the same cells stained with DAPI.

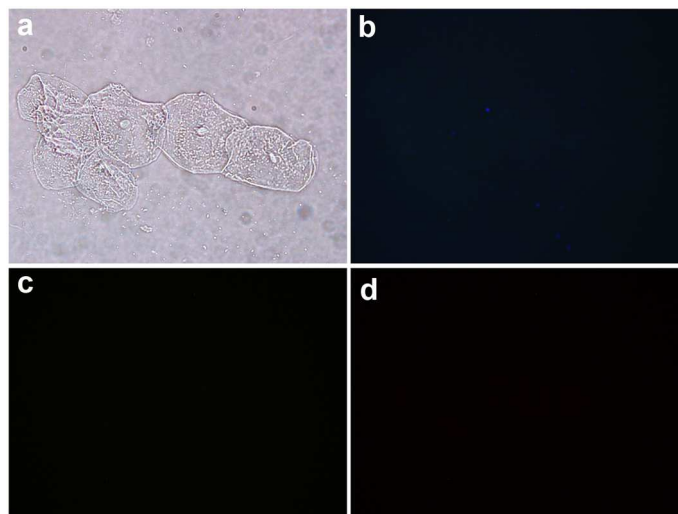


**Figure S13.** The fluorescence microscopic images of squamous epithelial cells non-treated with T-LSMO NPs: (a) bright field image; and fluorescence images collected upon excitation at (b) 365 nm, (c) 436 nm and (d) 546 nm wavelengths.

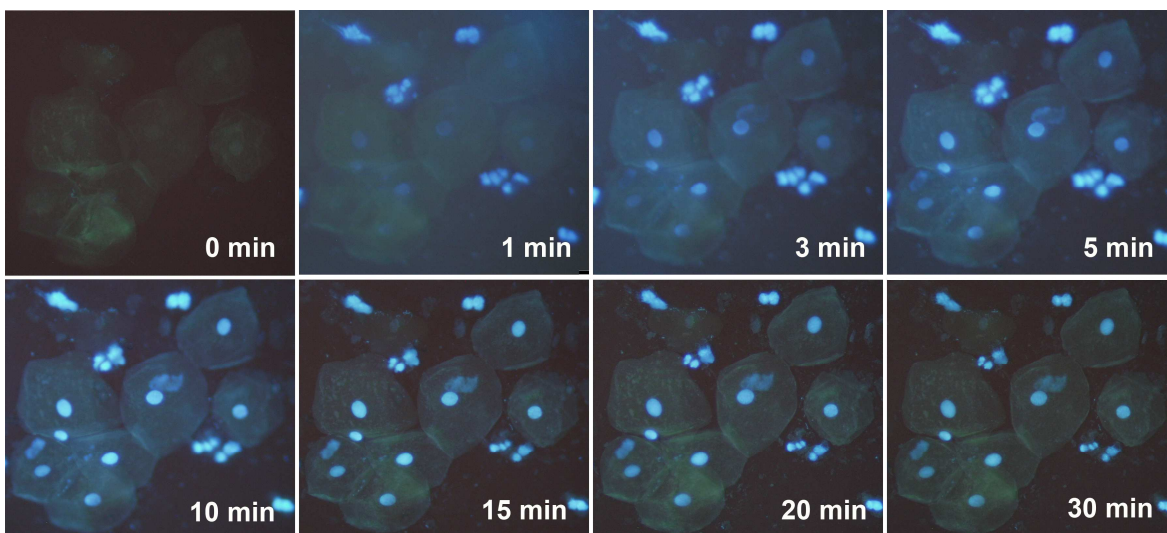


**Figure S14.** Time-dependent internalization of T-LSMO NPs into human oral squamous epithelial cells. Fluorescence micrographs (taken using an excitation source of 365 nm wavelength) of a single set of cells clearly indicates that the NPs become localized into to the nucleus of the cells within 30 min of addition.

**Table S1:** Spectral position of UV-vis absorption bands/peaks of tartrate, citrate and malate functionalized LSMO NPs along with their photoluminescence peak positions (except Malate-LSMO).

System	Positions of UV-vis absorption bands/peaks, $\lambda_{\text{abs}}$ (nm)	Position of photoluminescence peaks, $\lambda_{\text{em}}$ (nm)
T-LSMO	300, 440, 580 and 758	418, 470, 520 and 590
Citrate-LSMO	297, 430, 532 and 744	413, 479, 518 and 610
Malate-LSMO	304, 423, 526 and 746	Not been performed

## References

- (1) Coey, J. M. D.; Viret, M.; von Molnár, S. *Advances in Physics* **1999**, *48*, 167-293.
- (2) Verma, A.; Stellacci, F. *Small* **2010**, *6*, 12-21.
- (3) Daengsakul, S.; Thomas, C.; Thomas, I.; Mongkolkachit, C.; Siri, S.; Amornkitbamrung, V.; Maensiri, S. *Nanoscale Res. Lett.* **2009**, *4*, 839-845.